Materials & Design 240 (2024) 112829

Contents lists available at ScienceDirect

Materials & Design

journal homepage: www.elsevier.com/locate/matdes

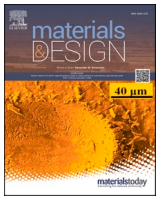

Hierarchical porous poly (L-lactic acid) fibrous vascular graft with controllable architectures and stable structure

Chen Meng [a], Jun Song [b], Samira Malekmohammadi [a], Jinmin Meng [a], Wenyuan Wei [a], Renzhi Li [a], Jiling Feng [c], R. Hugh Gong [a], Jiashen Li [a,*]

[a] Department of Materials, The University of Manchester, Manchester M1 7HL, UK
[b] Materdicine Lab, School of Life Sciences, Shanghai University, Shanghai 200444, China
[c] Department of Engineering, Manchester Metropolitan University, Manchester M15 6BH, UK

ARTICLE INFO

Keywords:
3D fibrous structure
Shape-controllable
Electrospinning
Poly(L-lactic acid)
Design for tubular scaffold

ABSTRACT

Electrospun fibre has shown great potential in tissue engineering and regenerative medicine due to its high specific surface area and extracellular matrix-mimicking structure. However, fabricating an electrospun fibrous scaffold with controllable complex 3D macroscopic configuration remains a challenge. In the present study, a novel method was designed to transform 2D electrospun poly (L-lactic acid) (PLLA) fibrous membrane to tubular PLLA fibrous scaffolds with 3D complex but tailored configuration. The electrospun PLLA fibrous membrane was rolled around a designed mould and then treated with acetone. Treated vascular grafts' length, diameter, and shape can be tailored by the mould parameters. Moreover, treated vascular grafts achieve favourable mechanical properties (Young's modulus = 155 MPa, tensile stress = 8.79 MPa and radial force = 2.2 N) and the mechanical properties could be engineered on demand. In addition, treated vascular grafts kept their initial structure and size during long-term *in vitro* experiments once they were formed. In addition, with the acetone-induced recrystallization of PLLA, pristine solid PLLA fibres were changed to hierarchical porous PLLA fibres with ultra-high specific surface area (28.9 m^2/g) and wettability (water contact angle = 101.32°), which has positive effects on cell adhesion and proliferation ability. A7r5 *in vitro* experiment shows that the proliferation rate of treated vascular grafts increased 153% at day 4 and 170.6% at day 7 compared with pristine vascular grafts.

1. Introduction

Cardiovascular disease is the leading cause of all deaths in the UK and globally [1]. The essential mechanism of cardiovascular disease is due to atherosclerosis developed in the artery, a slow and progressive build-up of fatty deposits (plaques) that cause narrowing or blockages of blood to the heart muscle or brain. Vascular graft for vascular disease is mainly for replacement of the diseased arteries or arteries bypass through open surgeries. Vascular scaffolds include autograft, allograft, and synthetic material tubes. However, using autogenous blood vessels requires a second operation that can cause harm to the patient's body. Also, due to insufficient harvesting or the patient's health, suitable autologous grafts are not always available [2]. Besides, the use of allografts is also limited due to the lack of tissue donors [3]. Therefore, artificial blood vessel implantation in situ is regarded as one of the best choices and developing tissue engineering vascular graft (TEVG) is a pressing requirement.

Tissue engineering is a strategy to fabricate TEVG. Its aim is the growth of extracellular matrix through seeding cells on synthetic scaffolds [4]. There are various methods for preparing tissue scaffolds, including self-assembly, template synthesis, phase separation, wet-spinning, and electrospinning. Tissue scaffolds prepared by nanofibrous materials are highly desirable as they can mimic the natural extracellular matrix (ECM) structure. Electrospinning enables the fabrication of fibres with diameters ranging from nanometres to micrometres, which have physical properties close to that of natural ECM [5]. Besides, electrospun fibrous scaffolds also have high porosity, good pore-interconnectivity and large surface areas [6]. Due to these advantages, electrospun fibre is an ideal material for fabricating in situ TEVG. Poly (L-lactic acid) (PLLA) is a renewable, bioresorbable, low-cost manufacturable synthetic material, that is approved for scaffold by the U.S. Food & Drug Administration and its counterparts in other countries [7,8]. It has been widely used in many fields such as tissue engineering scaffolds, food packaging, drug delivery systems, and many

* Corresponding author.
E-mail address: jiashen.li@manchester.ac.uk (J. Li).

https://doi.org/10.1016/j.matdes.2024.112829
Received 13 November 2023; Received in revised form 19 February 2024; Accepted 4 March 2024
Available online 11 March 2024

more [9].

Several groups have reported on the fabrication of vascular grafts using electrospun PLLA nanofibres. For example, Hashi and co-workers reported a vascular graft constructed from PLLA nanofibres. In this research, they constructed a PLLA electrospun vascular graft via a rotating mandrel and a longitudinally moving spinneret [10]. In another effort, Peng and co-workers fabricated a self-rolling PLLA and polycaprolactone bilayered vascular graft. The formation of a 3D tubular structure is created by the temperature-induced relaxation of intrinsic stress of electrospun PLLA fibrous membrane [11]. Although these two methods can fabricate PLLA electrospun vascular grafts, there are some limitations. Firstly, due to the different layers of the vascular grafts not being bonded with each other or the detachment of hollow tubes from the collector, cracks may occur on the fibres or general structure of vascular grafts. These issues may cause liquid leakage from the gaps under blood pressure [11,12]. Secondly, compared with commercial polyethene terephthalate vascular grafts, electrospun vascular grafts have less strength and elasticity [13]. Under low blood pressure, the electrospun vascular grafts always collapse after implantation as they do not have sufficient shape-retaining performance [14,15]. Lastly, in almost all previous studies, electrospun vascular grafts can only be prepared as simple straight tubular structures [12,16]. However, native blood vessels have complicated geometric structures, such as branch and tapered structures [17–19]. The ideal vascular grafts should include bifurcation structures and taper structures to better suit different patients as well as to minimize the vascular hemodynamic impairments to the physiological conditions, which can decrease the incidence of restenosis and thrombosis [20,21].

The current development of electrospun vascular grafts shows the following challenges: Firstly, electrospun vascular grafts require good structure integrity as well as higher mechanical properties and shape-retaining ability during and after the scaffold integration process; Secondly, electrospun vascular grafts should be able to mimic the geometric structures of real blood vessels instead being a simple tube. In our previous work, electrospun PLLA nanofibres were treated with acetone to generate a hierarchical porous structure. The mechanical properties of treated PLLA nanofibres also increased significantly [22,23]. Through further research, we found that PLLA nanofibres adhered together after the acetone treatment. These unique characteristics made it possible to develop an electrospun PLLA vascular graft. By our method, electrospun PLLA fibrous membranes were first collected and rolled around a designed mould. After that, they were treated with acetone. Through this method, acetone-treated vascular grafts have excellent structure integrity and mechanical properties. More than that, these grafts achieve various shapes, better cell adhesion and proliferation ability.

2. Materials and methods

2.1. Materials

PLLA (Mw = 1.43 × 10^6) was obtained from PURAC Biomaterials, Netherlands. Acetone (99.70%) and dichloromethane (DCM) (99.80%) were bought from Merck Life Science. Dimethylformamide (DMF, 99.80%) was bought from Fisher Scientific. Glass rods, needles, and ePTFE tubes were bought from VWR International and used as moulds. Ethanol was also bought from VWR International. The rat smooth muscle cell (SMC) line was purchased as A7r5 (ECACC 86050803) from the UK Health Security Agency. Dulbecco's modified eagle medium (DMEM D5796) was purchased from Sigma Aldrich.

2.2. Vascular graft fabrication

PLLA fibrous membranes were prepared based on a protocol published previously [22]. PLLA granules were dissolved by a dual-solvent system at 1.8 wt% concentration. The dual-solvents system included DCM and DMF at 19: 1 w/w. PLLA granules were added into DCM and stirred at 50 °C until all the PLLA was dissolved. After that, DMF was added dropwise into the solution. The electrospinning operation was conducted using an electrospinning unit by Tongli NanoTech. PLLA solution was transferred in a 20 ml Luer plastic syringe and loaded on a syringe pump. The injection speed was controlled at 5 ml/h during electrospinning. The distance between the nozzle tip and collector was kept at 20 cm and the voltage was set at 17 kV. Finally, the collected fibrous membrane was dried at room temperature in a fume hood for 24 h.

To prepare the vascular graft, electrospun PLLA fibrous membranes were cut into different rectangular strips by a scalpel. Then, these strips were manually rolled around various moulds. These moulds were sterilized by soaking in 75% ethanol for 1 h before use. After that, vascular grafts with moulds were immersed in acetone for 5 min and then dried in the fume hood for another 10 min. Lastly, all vascular grafts were gently detached from the moulds and stored in clean Petri dishes before further characterization. To fabricate the 6 mm diameter straight tubular vascular graft with different wall thicknesses, different lengths of PLLA fibrous membrane strips were prepared. In this research, 3 vascular graft samples with different wall thicknesses were prepared. All samples are prepared according to Table S1 and most of the characterizations were focused on these samples. Samples with different wall thicknesses before acetone treatment were named as pristine-thin, pristine-medium, and pristine-thick. Samples with different wall thicknesses after acetone treatment were named TEVG-thin, TEVG-medium, and TEVG-thick. All other vascular grafts including different diameter straight tubular vascular grafts and different shape vascular grafts were fabricated by rolling different length strips around glass rods, needles or designing ePTFE moulds.

2.3. Sample characterization

SEM: The surface morphology of the electrospun nanofibers and cross-section of the pristine and treated TEVG samples were observed using scanning electron microscopy (SEM, Zeiss Ultra-55) with an accelerating voltage of 1.5 kV.

Roughness: Surface roughness was tested by a laser optical microscope (μScan Nanofocus), a random 2 mm × 2 mm region from each sample was chosen to scan, and the resolution was set to 1 μm × 1 μm.

Mechanical properties: The tensile properties, radial compression, and shape memory ability of the pristine and treated TEVG samples were measured using a mechanical testing instrument (Instron Model 3344L). For the tensile test, the instrument was set to a tensile test mode. The samples were cut into 5 mm × 50 mm shapes and the extension speed was 5 mm/min. For radial compression and shape recovery tests, the instrument was set to a compression test mode. Samples of 20 mm long were held on a flat surface. A probe pressed the sample from above at a displacement rate of 5 mm/min. When the sample was pressed to about 50% of its original diameter, the pressing probe stopped and held for 10 s. After that, the probe was returned to the original place at the same rate as pressing.

Wettability: An optical contact angle equipment (Kruss DSA100) was used to calculate pristine and treated TEVG samples' surface water contact angle, with a controlled 20 μL of water per drop.

XRD: The crystallinity of pristine and treated TEVG samples was evaluated using an X-ray diffractometer (Panalytical XRD-5) with reflection mode Cu-Kα radiation and employing a scanning rate of 2°/min in a 2θ range from 10° to 40°.

DSC: Differential scanning calorimetry (TA Instrument Q-1000) was used for data acquisition. The temperature range was set from 20 °C to 200 °C with a heating rate of 10 °C/min. Each of the samples was measured three times, and the results were analyzed based on the average data.

BET: The specific surface area of pristine and treated TEVG samples was characterized by using a surface area analyzer (Micromeritics Gemini 2360).

Burst strength: The burst pressure of pristine and treated TEVG samples was measured by a self-designed apparatus consisting of a digital pump, a pressure sensor, and a sample holder. During testing, one end of the vascular graft sample was connected to a syringe loaded with PBS, and another end of the sample was connected to the pressure sensor. The PBS continued to be injected into the sample until it leaked, and the maximum pressure was recorded as the burst pressure. At least three replicates were measured for burst pressure.

In vitro incubation: To verify the hypothesis that the acetone post-treated TEVG can maintain a well-defined and regular shape for a long period, treated TEVG samples were incubated in PBS solution for 21 days, using pristine TEVG samples as controls.

2.4. SMCs in vitro experiment

A7r5 cells were cultured with about 15 ml of high glucose DMEM (D5796, Sigma Aldrich) supplemented with 10% fetal bovine serum and 1% antibiotics in a T75 flask. The flask was stored at 37 °C in a humidified air incubator containing carbon dioxide (5%). When cells reached over 90% confluency, they were trypsinized, harvested, washed, and re-suspended in DMEM medium [24]. 15 pristine TEVG samples and 15 treated TEVG samples were sterilized with 1 h exposure to UV light followed by a 5 min immersing with 70% ethanol solution. Then, all samples were washed with PBS buffer 3 times to remove ethanol. Subsequently, 60 μL cell suspension containing about $5x10^4$ cells was seeded on each sample. After an attachment window of 30 min of incubation, 1 ml cell culture medium was added for further growth in each well. The medium was changed every 3 days.

AlamarBlue® solution (BUF012, BIO-RAD) was used to perform a Resazurin Assay. The working solution was prepared by adding 10% AlamarBlue to the DMEM medium and keeping it from direct light exposure. At 1, 4, and 7 days, 6 samples including 3 pristine TEVG samples and 3 treated TEVG samples were selected for this assay. The old medium in each well was drained and rinsed with PBS solution. 1 ml working solution is added into the wells followed by 2 h of incubation along with blank solution. After incubation, 100 μL of working solution per sample was transferred to a sterilized 96-well plate 3 times, giving 9 trials for every sample. The same procedure was applied to the incubated blank solution as well. After that, the 96-well plate was sent to a microplate reader (BMG FLUOstar Omega) for fluorescence intensity detection.

Cell attachment, distribution status, and morphology were assessed by DAPI and phalloidin stain [25]. After 1, 4, and 7 days, cell-seeded samples were fixed using 10% neutral buffered formalin for 1 h. After removing the fixing solution, 0.1% Triton X-100 PBT solution was added to permeabilize the cell membrane. After that, samples were rinsed twice in PBS. Finally, the samples were stained with phalloidin for 1 h and then rinsed twice in PBS before being secondarily stained with DAPI for 5 min. The whole staining process was done under room temperature, and the dilution factor for phalloidin and DAPI was 1:1000 and 1:2000, respectively. Images were obtained on a laser confocal microscopy (Leica TCS SP8).

2.5. Statistical analysis

All data were expressed as mean ± standard deviation. Statistical differences between different samples were evaluated by T-test in Excel. All data were analyzed by Origin 2018 software. The vascular graft's wall thickness was measured by ImageJ using SEM images. Cell number was calculated by using QuPath software according to the DAPI stain results.

3. Result and discussion

3.1. Surface morphology

In this research, a binary solvent system, including DCM and DMF, was used. DCM is a solvent and DMF is a non-solvent of PLLA. During electrospinning, the fast evaporation of DCM could cause phase separation between the polymer (PLLA) and the non-solvent (DMF). After the remained DMF was completely evaporated from the fibres, its regions were left as pores or pits on the fibre surface as shown in Fig. 1a and b [26]. In addition, when the electrospun fibres reached the collector, due to the low solution concentration (1.8%), they were only half-dried with a soft polymer shell and some solvents inside the fibres. Meanwhile, the PLLA shell was not hard enough to maintain the round fibre shape [22]. Therefore, some fibres became flat, as shown in Fig. 1b. Moreover, for the pristine TEVG surface, all PLLA fibres are mutually independent with less crosslinking between them. Therefore, the pristine TEVG sample surface is very fluffy, as shown in Fig. 1b.

After acetone post-treatment, PLLA fibres on the treated TEVG sample surface show a hierarchical porous structure, which is significantly different from the pristine sample surface morphology. The reason for this change is that acetone could recrystallize PLLA polymer chains. To be specific, as the solvent evaporates very fast during electrospinning, electrospun PLLA fibres are mostly in an amorphous state after reaching the collector. When PLLA fibres were immersed in acetone, acetone infiltrated quickly into the amorphous phase of PLLA and swelled the whole fibres. Therefore, amorphous PLLA chains were rearranged by solvent-induced recrystallization [27,28]. At the same time, numerous nano-pores were formed among the whole polymer fibre. Finally, the electrospun PLLA fibres were transferred from solid fibres to hierarchical porous ones. Moreover, the flat ribbon-shaped fibres recovered to be round, as shown in Fig. 1d and f. With a hierarchical porous fibrous structure, treated TEVG samples have an ultra-high specific surface area of 28.986 m^2/g, significantly higher than pristine TEVG (3.716 m^2/g), as shown in Fig. S2. Further, there is obvious crosslinking between PLLA fibres after acetone post-treatment (Fig. 1c). PLLA fibres adhered together during solvent-induced recrystallization [26]. With this crosslinking, the treated TEVG sample surface became more compact and had lower general surface roughness than the fluffy pristine TEVG sample surface (Fig. S1). In conclusion, treated TEVG samples with hierarchical porous PLLA fibres have higher surface area and porous fibre structure which can absorb and retain more protein and nutrients. It is beneficial for cell attachment and proliferation.

Fig. 1c and f show the cross-sectional morphology of the pristine-medium sample and TEVG-medium sample (other images for the cross-sectional morphology of pristine-thin, TEVG-thin, pristine-thick, and TEVG thick samples are shown in Fig. S3). The pristine-medium sample shows a loose inter-layer structure. Clear inner cavities could be observed between different rolling layers without cross-linking. After acetone post-treatment, as the adjacent rolling layers were merged, there were no inner cavities on the TEVG-medium sample's cross-section.

3.2. Acetone post-treatment mechanism

During the acetone treatment, as PLLA and acetone have similar Hansen solubility, PLLA fibres were strongly swollen by acetone providing more free spaces for polymer chains. The swelling degree of PLLA could be up to 150% [29]. The stretched polymer chains relaxed and shrunk during acetone treatment, which could shorten the length of PLLA fibre, resulting in a significant overall contraction of the PLLA fibrous membrane [23]. Fig. 2c shows the force change on the PLLA fibrous membrane while it was immersed in acetone at room temperature. Initially, as the PLLA fibres were swollen by acetone and polymer chains relaxed, the membrane expanded rapidly. After that, the rearrangement of polymer chains gave a shrinkage force to the fibrous

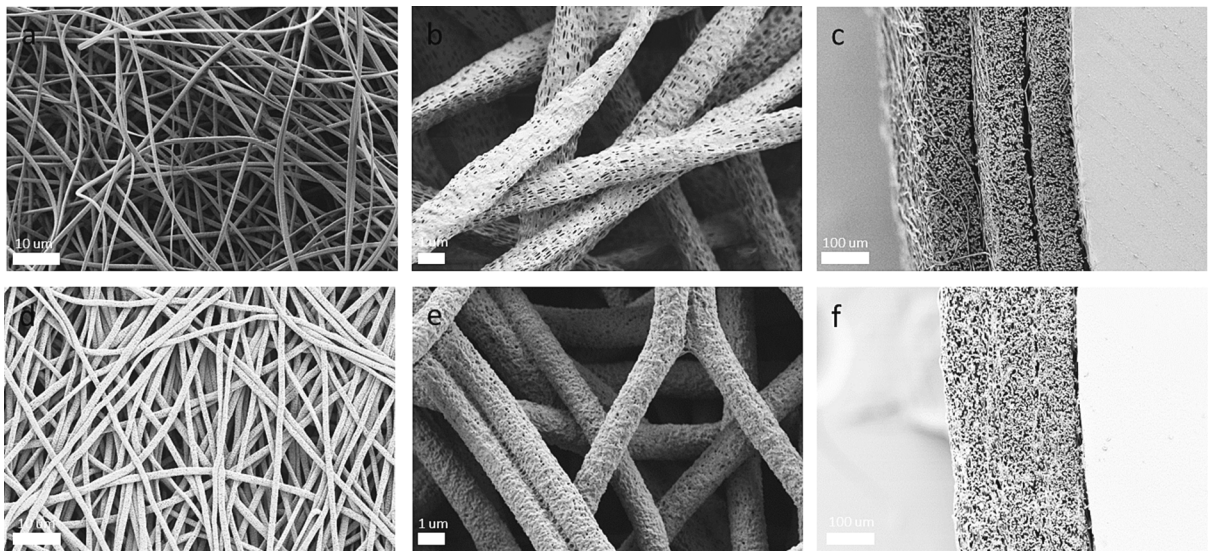

Fig. 1. SEM images of pristine TEVG samples and TEVG samples. a) Pristine TEVG samples (low magnification); b) Pristine TEVG samples (high magnification); c) Cross-section of pristine TEVG samples; d) Acetone-treated TEVG samples (low magnification); e) Acetone-treated TEVG samples (high magnification); f) Cross-section of acetone-treated TEVG samples.

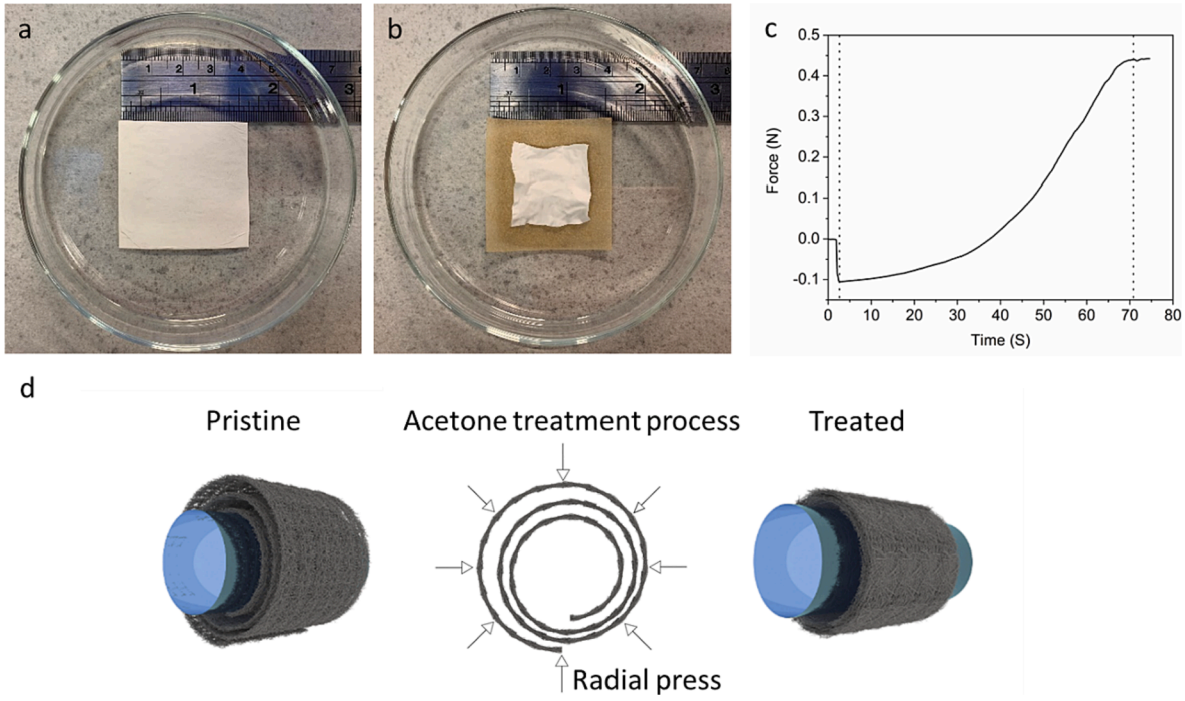

Fig. 2. a,b) Electrospun PLLA fibrous membrane's change after acetone treatment; c) Shrinkage force during acetone treatment; d) Mechanism of acetone treatment.

membrane. The maximum shrinkage force was about 0.54 N on a 5 mm width rectangular stripe. Pristine PLLA fibrous membrane shrunk about 50% after acetone post-treatment (Fig. 2a and b). When a vascular graft was fabricated, a piece of electrospun PLLA fibrous membrane was rolled around a glass rod. Then the rolled membrane with the glass rod was immersed in acetone. The shrinkage force was changed to be a radial pressure to press the multi layers on the glass rod (Fig. 2d). Generally, for PLLA with lower Mw, acetone works as a solvent for PLLA [30]. However, for PLLA with ultra-high Mw (Mw = 1.43×10^6), acetone can only swell and slightly dissolve PLLA fibres. After acetone was completely evaporated, fibres were adhered together by those slightly dissolved PLLA. Due to the adhesion of PLLA fibres and a radial pressure caused by the rearrangement of polymer chains, fluffy PLLA fibres became compact on TEVG samples after acetone treatment. Consequently, the outer diameter and thickness of the TEVG samples were smaller than the pristine samples after acetone treatment (Fig. S4). By this method, the final TEVG had excellent structural integrity.

3.3. Materials properties

3.3.1. Water contact angle

PLLA is a kind of hydrophobic polymer. With a fluffy surface, the pristine samples had a higher water contact angle at 138.4° [26,31]. However, after acetone treatment, the treated TEVG sample's water contact angle was reduced to 101.3° (Fig. 3a). The big difference in hydrophilicity before and after acetone treatment was caused by the

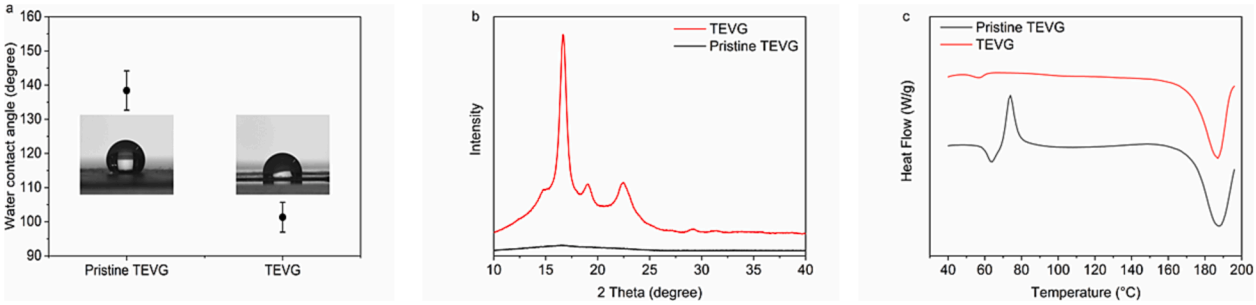

Fig. 3. a) Water contact angle results; b) XRD results; c) DSC results.

change in surface roughness and porosity [32,33]. Acetone-treated surface became compact and smooth. The average roughness of the pristine sample was 2.631 μm. After acetone treatment, the average roughness of the TEVG sample reduced to 0.857 μm. Therefore, the water contact angle decreased and treated TEVG samples became a little bit hydrophilic after acetone treatment. Generally, treated TEVG samples with improved hydrophilic properties are advantageous for cellular nutrient supply, cell adhesion, growth, and waste removal.

3.3.2. XRD

During the electrospinning process, polymer molecule chains are stretched while the charged jet of the polymer fluid is elongated by the electric field. Meanwhile, the solvent evaporates quickly, leaving behind a polymer fibre with stretched polymer chains. As this process happens in a very short time, it leaves not enough time for an orderly molecular chain arrangement. Therefore, most of the electrospun PLLA fibres are still amorphous with low crystallinity [27,34]. Fig. 3b shows the XRD result of pristine TEVG and treated TEVG samples. Firstly, for the pristine TEVG samples, only a wide weak peak at about 16.9° was detected, which means that PLLA fibres were in a low crystallization status. Compared with previous research [22,24], there is no difference in the XRD results between electrospun PLLA fibres and PLLA fibres from pristine TEVG samples. This shows that the hand-rolling process didn't change the crystallinity of the PLLA fibres. After acetone treatment, four peaks were observed in the XRD graph. The most remarkable peak of treated TEVG samples is at about 16.9°, which refers to the (200/110) plane [35]. Moreover, the other three relatively weak peaks located at 14.7°, 19.0°, and 22.3° are referred to as (010), (203) and (015) planes, respectively. Considering the crystallization conditions, PLLA fibres were crystallized into α formation [22,27].

3.3.3. DSC

The DSC results are exhibited in Fig. 3c. For pristine TEVG samples, peaks of glass transition temperature [36], cold crystallization temperature (Tcc), and melting crystalline phase were obvious, which were noted at 58 °C, 74 °C, and 180 °C, respectively [22]. It is proposed that the Tcc of the pristine TEVG sample corresponds to the amorphous state of polymer chains having mobility above their Tg and recrystallization. After acetone treatment, treated TEVG samples' peak of Tcc disappeared, indicating their higher crystallinities. The DSC results also matched those of XRD, further confirming the increased degree of crystallinity after treatment.

3.4. Mechanical properties

The tensile test results are shown in Fig. 4a, and b. The data are shown in the bar chart (Fig. 4c). The ultimate tensile stresses of pristine TEVG samples were 3.13 MPa (pristine-thick), 2.78 MPa (pristine-medium) and 2.49 MPa (pristine-thin) with a similar elongation value of about 60%. It is observed that all pristine TEVG samples have relatively lower mechanical properties. Although Young's modulus and tensile stress of the different pristine PLLA samples increased with the change in wall thickness, the increment was not significant. However, after acetone treatment, all TEVG samples exhibited better mechanical

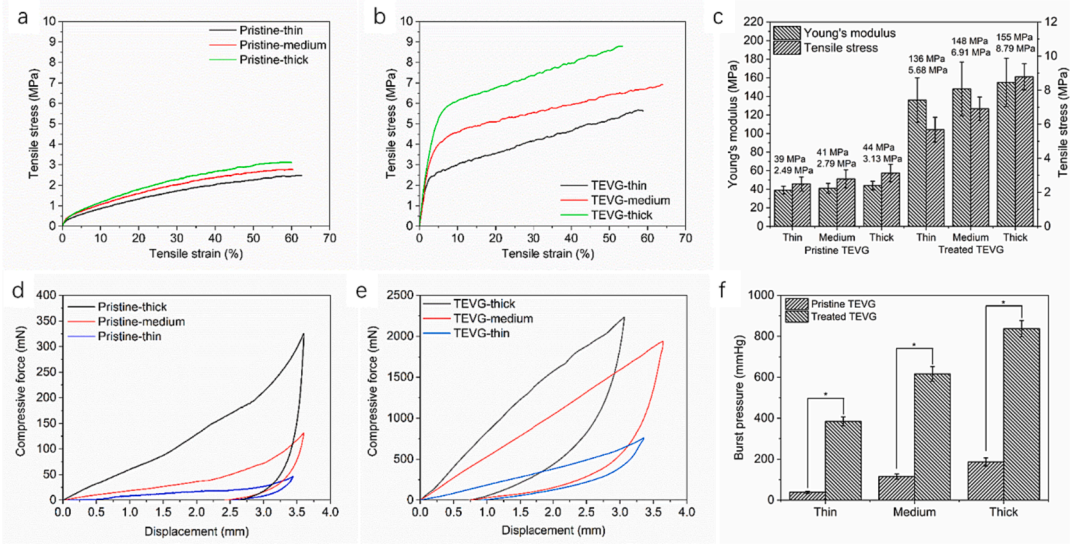

Fig. 4. a) Tensile test results of pristine TEVG samples. b) Tensile test results of TEVG samples. c) Young's modulus and tensile stress of pristine TEVG and TEVG samples. d) Compress force and recovery of pristine TEVG samples. e) Compress force and recovery of TEVG samples. f) Burst pressure of pristine TEVG and TEVG samples. "*" represents the significance of the *t*-test ($p < 0.05$).

properties than pristine samples, with the tensile strengths increased to 8.79 MPa (TEVG-thick), 6.91 MPa (TEVG-medium), and 5.67 MPa (TEVG-thin). Firstly, after acetone treatment, TEVG samples show higher crystallinity which increases the rigidness of the PLLA fibres on treated TEVG samples. Secondly, the treated TEVG samples with different wall thicknesses showed different shrinkage degrees. Therefore, unlike the pristine TEVG samples, different TEVG samples had obvious differences in tensile strength So, it is convenient to meet mechanical requirements by changing the number of layers. For example, native blood vessels have various mechanical properties, such as the human internal mammary artery (tensile stress and elongation to break are 4.3 MPa and 59%), human saphenous vein (tensile stress and elongation to break are 6.3 MPa and 17%), and human femoral artery (tensile stress and elongation to break are 1–2 MPa and 63–76%) [37–39]. In this study, the treated TEVG samples can be tailored to mimic the mechanical properties of native vessels according to the specific needs of different patients. This allows them to withstand hemodynamic forces both immediately upon implantation and over the long term, while also remaining resistant to permanent deformation that could potentially lead to aneurysm formation [40].

The results of radial compressive and shape-retaining ability are given in Fig. 4d and e. Pristine samples showed lower radial compressive force with 0.27 N (pristine-thick), 0.13 N (pristine-medium), and 0.035 N (pristine-thin) and all pristine samples showed almost no shape-retaining ability. Pristine TEVG samples were prone to collapse and had a lower ability to recover from deformation (Fig. S5a–c). After acetone treatment, the resistance to radial deformation of treated TEVG samples increased sharply (p-value < 0.05), with 2.2 N (TEVG-thick), 1.9 N (TEVG-medium), and 0.8 N (TEVG-thin). In addition, the shape-retaining ability of treated TEVG samples showed a significant improvement as the shape recovery ratio of TEVG samples was about 70%-80%. Treated TEVG samples could restore their original shape almost completely after being pressed (Fig. S5d–f) [41]. After acetone post-treatment, PLLA fibres have a higher degree of crystallinity, which increases the stiffness and elastic modulus of the TEVG samples. Therefore, TEVG samples have better circular shape-maintaining properties. In vascular design and development, the artificial blood vessel always suffers a collapse after implantation such as the right ventricular outflow tract, and collapsing of vascular walls can cause immediate clogging [14,42,43]. Previous research about electrospun fibrous vascular grafts does not provide sufficient shape memory performance in small-diameter arterial substitutes and venous prostheses of any diameter. Thus, electrospun vascular grafts with improved radial compressive force and shape-retaining ability should be privileged [15].

The burst pressure measurement was carried out using PBS. The maximum pressure that caused PBS leakage was recorded as the burst pressure since it indicated the failure of the graft. All results are shown in Fig. 4f. It was found that the treated TEVG samples had much higher burst pressure than the pristine TEVG samples. This was because after acetone treatment, the adjacent rolling layers were adhered together and there was no gap between them. In this situation, there was no PBS leakage under low pressure. The treated TEVG samples showed the highest burst pressure of about 840 mmHg, which was still lower than native saphenous veins. This was because PBS liquid was easy to penetrate the highly porous structure of electrospun PLLA grafts under pressure. Although the TEVG samples' burst pressure was lower than native saphenous veins, normal blood pressure is 120/80 mmHg, and maximum blood pressure for hypertension patients is 180 mmHg [44]. Thus, the burst pressure of the TEVG samples developed in this study should be high enough to bear the native hemodynamic load [45].

3.5. Structural stability

To verify the hypothesis that TEVG after acetone treatment can maintain a well-defined and regular structure for a long period. Pristine TEVG samples and treated TEVG samples were incubated in 50 ml PBS in a shake incubator. The temperature was set at 37 °C with a rotational speed of 80 rpm. At the beginning of the incubation, the pristine TEVG samples and the TEVG samples all showed regular and compact structures. After 1 day of incubation, the pristine TEVG's structure tended to collapse (Fig. S6a and b). Pristine TEVG gradually swelled. Part of the fibrous membrane recovered to a flat stripe because there is no physical crosslinking between adjacent layers. However, for treated TEVG, the inner diameter and general structure remained constant without layer detachment. Fig. 5a, b, and c show SEM images of the treated TEVG sample's cross-section after 7 days, 14 days, and 21 days of incubation. Compared with the cross-section morphology in Fig. 1f, all the sample cross sections are still tightly bonded without any inner cavities, and the wall thickness also doesn't show obvious change. Moreover, the digital images also show that the TEVG sample maintains well general structure after long-term *in vitro* incubation (Fig. S6). When attempts were made to unroll the scaffolds by hand, a strong adhesive force was felt between PLLA fibres. These results strongly demonstrate that TEVG samples have good structural stability. With good structural stability, the treated samples could show excellent shape maintenance and good patency after implantation, demonstrating the promising potential of this study in blood vessel engineering.

Immersing the sample in PBS or equivalent buffer solution at 37 °C is a common method for the assessment of polymer degradation [46]. No significant morphological changes were observed after 4 days of incubation despite some small breakdowns on PLLA fibres. After 10 days of degradation, the fibres started to break down into small pieces (Fig. S7). Although PLLA fibres break down, the treated TEVG sample maintains well general structure, as mentioned above. Therefore, the treated TEVG samples could maintain original shape during degradation. More than that, after 4-, 7- and 10-days degradation, the treated TEVG samples could also maintain their mechanical performance (Fig. S8).

3.6. Variable shape

Various 3D complex configurations of fibrous tubular structures could be fabricated by this method, including straight tubes with different inner diameters, and bifurcated, and tapered macrostructures, as shown in Fig. 5d to 5f. The fabricated 3D fibrous vascular grafts accurately replicated the expected parameters of the mould used. The replication quality of the tubular scaffold produced through this moulding-assisted acetone treatment is expected to be maintained until the feature size decreases to less than 1 mm. Although several research reported electrospinning with 3D collectors to fabricate complex fibrous tubular structures, there are still several difficulties. Firstly, collecting fibrous tubes from the collector may result in the occurrence of cracks in the fibrous structures. Secondly, as a collector with a complex structure is prone to the accumulation of electric charges during electrospinning, it is difficult to prepare small complex fibrous tubes. Thirdly, the 3D electrospinning collectors are expensive and difficult to fabricate [18,47,48]. In this study, the fabrication method could significantly increase the degree of freedom in designing a 3D nanofibrous macrostructure. Firstly, after acetone treatment, the fluffy cotton-like fibrous structure becomes compact with higher mechanical strength, and the 3D moulds are easily removed [49]. Secondly, 3D moulds are more cost-effective and readily available for purchase or fabrication. Accordingly, various fibrous tubular macrostructures could be fabricated by this method to mimic the 3D configurations and sizes of native vascular networks [50]. In addition, this method could easily fabricate 3D fibrous multi-bifurcated and/or curvilinear tubular structures, broadening the utilization of fibrous tissue scaffolds [51].

3.7. Cell proliferation ability

Laser confocal images were employed to show details of the cell shape and distribution at three time points after cell culture, as shown in Fig. 6a–f. For clear observation, the cells were stained by both DAPI and

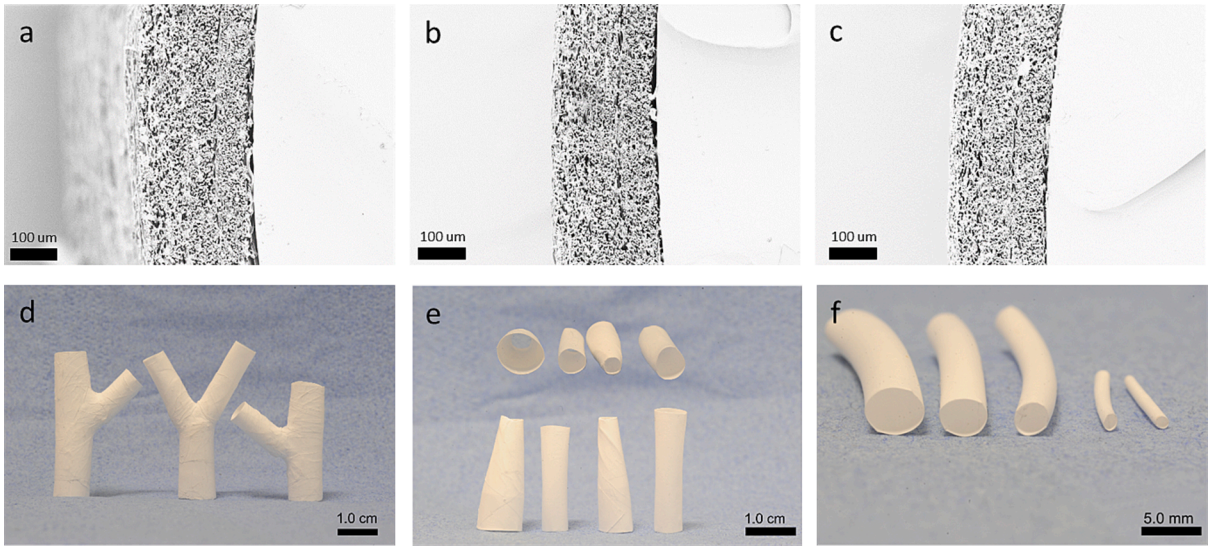

Fig. 5. a-c) Cross-section morphology of treated TEVG after 7-day, 14-day and 21-day incubation in PBS, these pictures illustrate the TEVG samples' excellent structure integrity; d) Images of bifurcated treated TEVG samples; e) Images of straight and tapered treated TEVG samples; f) Images of different inner diameters treated TEVG samples.

Phalloidin. Cell nuclei were navigated by DAPI, and cell cytoskeleton was conjugated by Phalloidin to examine cell density and morphology [52]. After 1 day of culturing, the cells exhibited rounded morphology on the pristine TEVG while some cells that are attached to the TEVG spread and exhibit a flat morphology. Cells on the pristine TEVG samples exhibited a rounded morphology with few filopodia indicating that most cells were poorly adhered to the sample surface. In contrast, cells cultured on treated TEVG samples exhibited stretched cytoskeleton and filopodia indicating genuine adhesion of the cells to the sample surface. As time progressed, although increases in cell density could be observed in both pristine TEVG and treated TEVG samples, the number and spreading of cells appeared greater in the treated TEVG samples compared with the pristine TEVG samples. These differences are due to the hierarchical porous fibre structure on the treated TEVG samples enhancing cell attachment and proliferation in comparison to solid and smooth fibre structure on the pristine TEVG samples [53]. What's more, the enhancement in wettability and structural integrity may also benefit cell attachment and viability during cell seeding [26].

To investigate the cell proliferation rate of pristine TEVG samples and treated TEVG samples, Alamar blue assay and cell number were examined. Alamar blue assay could directly investigate the proliferation rate of viable cells grown on the samples at each time point as this method detects the metabolism reaction via monitoring the fluorescence intensity (FI) from oxidation-reduction reactions toward growth medium [26,54]. The assay result is shown in Fig. 6g. Regarding the test results, the cellular metabolic activity of the A7r5 cell increased with the culture time for both pristine TEVG and TEVG samples, indicating that they were both non-cytotoxic and able to support smooth muscle cell adhesion and growth. More importantly, as the FI value is proportional to the number of metabolically active cells, treated TEVG samples showed higher FI values than pristine TEVG samples, which indicated that TEVG samples had better cellular biocompatibility [25]. The cell count test on day 1 (24 h after seeding) evaluated the cell adhesion rate (CAR) of A7R5 cells on pristine and treated TEVG samples (Fig. 6h). According to the result, CAR for the TEVG samples was better than that of the pristine TEVG samples. Furthermore, there were more cells on TEVG samples than on pristine TEVG samples after 4 days and 7 days of culturing. The average increments of cell number on treated TEVG samples were 74.6% at day 4 and 253.8% at day 7. These results suggested that treated TEVG samples had better cellular biocompatibility, more cell attachment and proliferation than pristine TEVG samples. These improvements could be attributed to the treated TEVG samples having higher specific surface area as well as higher wettability which could absorb and retain more protein and nutrients in the culture medium.

3.8. *Limitations and future work*

Firstly, blood compatibility tests are being planned in the future. Secondly, more in-depth biological experiments such as cell infiltration, functional validation, and endothelial cell evaluation, as well as *in vivo* studies, are also directions for future research.

4. Conclusion

In conclusion, a rapid and facile strategy has been developed to fabricate vascular grafts using biodegradable electrospun PLLA fibrous membranes and acetone treatment. By designing different 3D moulds, cell-free vascular grafts with different macroscopic configurations (length, diameter, shape) can be fabricated. Furthermore, this method does not rely on any complex equipment, manipulations, and moulds. After acetone treatment, PLLA vascular grafts are recrystallized to be a highly porous structure with enhanced mechanical properties. Moreover, by changing the initial layer numbers or wall thickness during the fabrication process, the final vascular graft's tensile strength and/or compressive strength and/or burst pressure could be engineered on demand. This method provides a rapid tool to fabricate tailored tubular scaffolds with designed architectures and mechanical properties. The 7-day *in vitro* cell culture with smooth muscle cells revealed that acetone-treated TEVG samples with highly specific surface area and wettability have better cell adhesion and proliferation performance. Due to these advantages, this method provides attractive opportunities in the design and fabrication not only for vascular grafts but also for other 3D fibrous tubular scaffolds such as nerves, oesophagus, and urethra. This novel method has significant potential for the development of tubular scaffolds.

CRediT authorship contribution statement

Chen Meng: Writing – review & editing, Writing – original draft, Methodology, Investigation, Formal analysis, Conceptualization. **Jun Song:** Writing – review & editing, Methodology. **Samira**

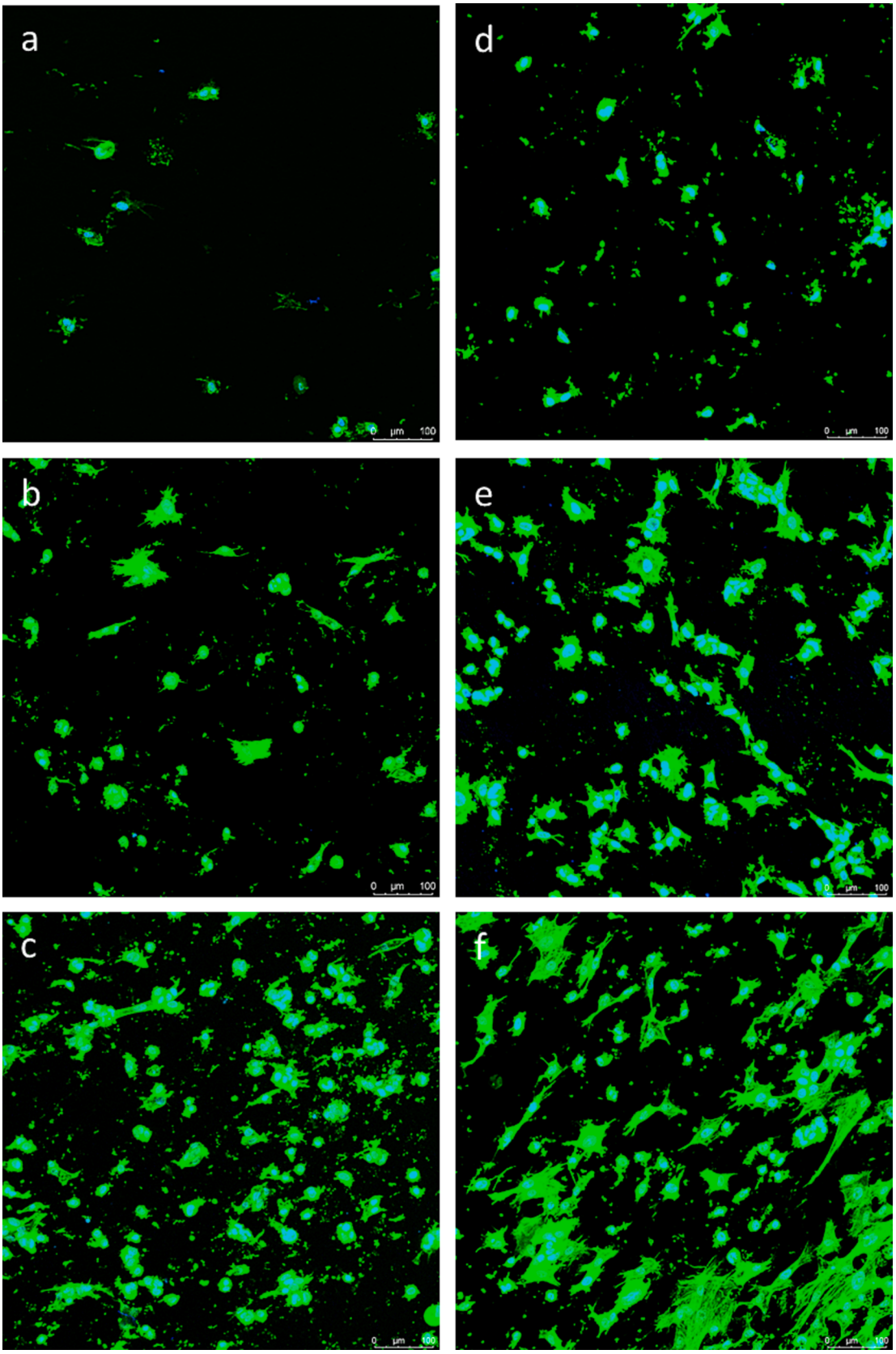

Fig. 6. a-c) The morphology of cells growing on the pristine TEVG samples after 1 day, 4 days, and 7 days culturing; d-f) The morphology of cells growing on the TEVG samples after 1 day, 4 days, and 7 days culturing; g) Alamar blue assay results; h) Cell number counts. "**" represents the significance of the *t*-test ($p < 0.05$). (For interpretation of the references to colour in this figure legend, the reader is referred to the web version of this article.)

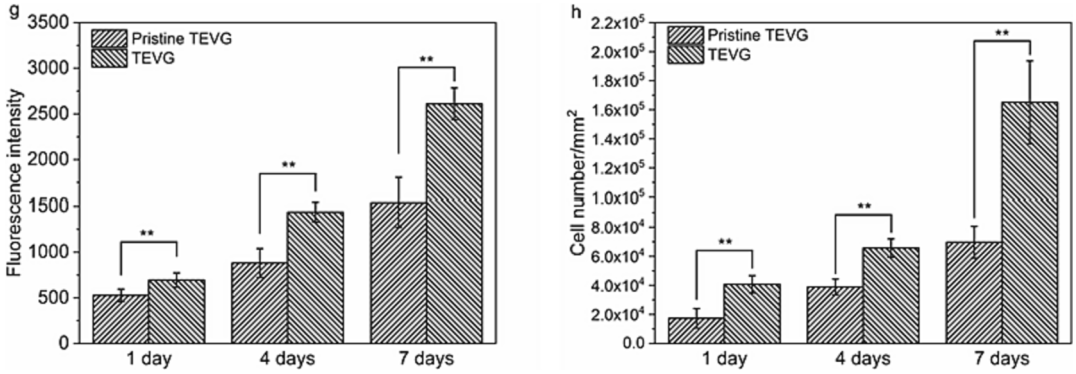

Fig. 6. (*continued*).

Malekmohammadi: Writing – review & editing. **Jinmin Meng:** Formal analysis. **Wenyuan Wei:** Formal analysis. **Renzhi Li:** Formal analysis. **Jiling Feng:** Writing – review & editing. **R. Hugh Gong:** Writing – review & editing. **Jiashen Li:** Writing – review & editing, Supervision, Conceptualization.

Declaration of Competing Interest

The authors declare that they have no known competing financial interests or personal relationships that could have appeared to influence the work reported in this paper.

Data availability

Data will be made available on request.

Acknowledgements

The authors would like to thank Stuart Morse in the Department of Materials at the University of Manchester for his help with mechanical testing. The authors also acknowledge the support of the Electron Microscopy Centre, XRD suite and Henry Royce Institute at The University of Manchester. Dr Jun Song is sponsored by the Shanghai Pujiang Program (22PJD026).

Appendix A. Supplementary data

Supplementary data to this article can be found online at https://doi.org/10.1016/j.matdes.2024.112829.

References

[1] A.S. Update, Heart disease and stroke statistics–2017 update, Circulation 135 (2017) e146–e603.
[2] D. Wang, Y. Xu, Q. Li, L.-S. Turng, Artificial small-diameter blood vessels: materials, fabrication, surface modification, mechanical properties, and bioactive functionalities, J. Mater. Chem. B 8 (9) (2020) 1801–1822.
[3] A. Hasan, A. Memic, N. Annabi, M. Hossain, A. Paul, M.R. Dokmeci, F. Dehghani, A. Khademhosseini, Electrospun scaffolds for tissue engineering of vascular grafts, Acta Biomater. 10 (1) (2014) 11–25.
[4] N.K. Awad, H. Niu, U. Ali, Y.S. Morsi, T. Lin, Electrospun fibrous scaffolds for small-diameter blood vessels: a review, Membranes 8 (1) (2018) 15.
[5] A. Ndreu, L. Nikkola, H. Ylikauppila, N. Ashammakhi, V. Hasirci, Electrospun Biodegradable Nanofibrous Mats for Tissue Engineering, 2008.
[6] S. Agarwal, J.H. Wendorff, A. Greiner, Progress in the field of electrospinning for tissue engineering applications, Adv. Mater. 21 (32–33) (2009) 3343–3351.
[7] T. Xu, H. Yang, D. Yang, Z.-Z. Yu, Polylactic acid nanofiber scaffold decorated with chitosan islandlike topography for bone tissue engineering, ACS Appl. Mater. Interfaces 9 (25) (2017) 21094–21104.
[8] C. Ru, F. Wang, M. Pang, L. Sun, R. Chen, Y. Sun, Suspended, shrinkage-free, electrospun PLGA nanofibrous scaffold for skin tissue engineering, ACS Appl. Mater. Interfaces 7 (20) (2015) 10872–10877.
[9] R. Mehta, V. Kumar, H. Bhunia, S. Upadhyay, Synthesis of poly (lactic acid): a review, J. Macromol. Sci, C Polym. Rev. 45 (4) (2005) 325–349.
[10] C.K. Hashi, N. Derugin, R.R.R. Janairo, R. Lee, D. Schultz, J. Lotz, S. Li, Antithrombogenic modification of small-diameter microfibrous vascular grafts, Arterioscler. Thromb. Vasc. Biol. 30 (8) (2010) 1621–1627.
[11] L. Peng, J. Zhu, S. Agarwal, Self-rolled porous hollow tubes made up of biodegradable polymers, Macromol. Rapid Commun. 38 (10) (2017) 1700034.
[12] N. Wang, L. Tang, W. Zheng, Y. Peng, S. Cheng, Y. Lei, L. Zhang, B. Hu, S. Liu, W. Zhang, A strategy for rapid and facile fabrication of controlled, layered blood vessel-like structures, RSC Adv. 6 (60) (2016) 55054–55063.
[13] L. Ye, X. Wu, Q. Mu, B. Chen, Y. Duan, X. Geng, Y. Gu, A. Zhang, J. Zhang, Z.-G. Feng, Heparin-conjugated PCL scaffolds fabricated by electrospinning and loaded with fibroblast growth factor 2, J. Biomater. Sci. Polym. Ed. 22 (1–3) (2011) 389–406.
[14] Y. Fu, R. Guidoin, R. De Paulis, J. Lin, B. Li, L. Wang, M. Nutley, D. Desaulniers, Z. Zhang, The Gelweave Valsalva graft to better reconstruct the anatomy of the aortic root, J. Long Term Eff. Med. Implants 26 (2) (2016).
[15] C. Li, F. Wang, P. Chen, Z. Zhang, R. Guidoin, L. Wang, Preventing collapsing of vascular scaffolds: the mechanical behavior of PLA/PCL composite structure prostheses during in vitro degradation, J. Mech. Behav. Biomed. Mater. 75 (2017) 455–462.
[16] P. Wu, N. Nakamura, H. Morita, K. Nam, T. Fujisato, T. Kimura, A. Kishida, A hybrid small-diameter tube fabricated from decellularized aortic intima-media and electrospun fiber for artificial small-diameter blood vessel, J. Biomed. Mater. Res. A 107 (5) (2019) 1064–1070.
[17] Y. Yu, Y. Zhou, Q. Ma, S. Wu, Y. Sun, X. Liu, Y. Zhao, Y. Liu, D. Shi, The conical stent in coronary artery improves hemodynamics compared with the traditional cylindrical stent, Int. J. Cardiol. 227 (2017) 166–171.
[18] S.R. Jang, J.I. Kim, C.H. Park, C.S. Kim, Development of Y-shaped small diameter artificial blood vessel with controlled topography via a modified electrospinning method, Mater. Lett. 264 (2020) 127113.
[19] X.Q. Dong, Y.L. Li, X. Ding, L. Wang, Research on the manufacture of tapered artificial vascular, Adv. Mat. Res. 331 (2011) 512–515.
[20] R. Tejeda-Alejandre, H. Lara-Padilla, C. Mendoza-Buenrostro, C.A. Rodriguez, D. Dean, Electrospinning complexly-shaped, resorbable, bifurcated vascular grafts, Procedia CIRP 65 (2017) 207–212.
[21] F. Meng, Y. Li, Automatic formation techniques and uniformity evaluation of conical vascular graft, 47Textile Res. (2019) 110.
[22] Z. Lu, B. Zhang, H. Gong, J. Li, Fabrication of hierarchical porous poly (l-lactide) (PLLA) fibrous membrane by electrospinning, Polymer 226 (2021) 123797.
[23] J. Song, B. Zhang, Z. Lu, Z. Xin, T. Liu, W. Wei, Q. Zia, K. Pan, R.H. Gong, L. Bian, Hierarchical porous poly (l-lactic acid) nanofibrous membrane for ultrafine particulate aerosol filtration, ACS Appl. Mater. Interfaces 11 (49) (2019) 46261–46268.
[24] J. Song, Z. Chen, L.L. Murillo, D. Tang, C. Meng, X. Zhong, T. Wang, J. Li, Hierarchical porous silk fibroin/poly (L-lactic acid) fibrous membranes towards vascular scaffolds, Int. J. Biol. Macromol. 166 (2021) 1111–1120.
[25] Z. Lu, W. Wang, J. Zhang, P. Bártolo, H. Gong, J. Li, Electrospun highly porous poly (L-lactic acid)-dopamine-SiO2 fibrous membrane for bone regeneration, Mater. Sci. Eng. C 117 (2020) 111359.
[26] C. Meng, D. Tang, X. Liu, J. Meng, W. Wei, R.H. Gong, J. Li, Heterogeneous porous PLLA/PCL fibrous scaffold for bone tissue regeneration, Int. J. Biol. Macromol. 235 (2023) 123781.
[27] J. Gao, L. Duan, G. Yang, Q. Zhang, M. Yang, Q. Fu, Manipulating poly (lactic acid) surface morphology by solvent-induced crystallization, Appl. Surf. Sci. 261 (2012) 528–535.
[28] N. Naga, Y. Yoshida, M. Inui, K. Noguchi, S. Murase, Crystallization of amorphous poly (lactic acid) induced by organic solvents, J. Appl. Polym. Sci. 119 (4) (2011) 2058–2064.
[29] S. Sato, D. Gondo, T. Wada, S. Kanehashi, K. Nagai, Effects of various liquid organic solvents on solvent-induced crystallization of amorphous poly (lactic acid) film, J. Appl. Polym. Sci. 129 (3) (2013) 1607–1617.
[30] R. Casasola, N.L. Thomas, A. Trybala, S. Georgiadou, Electrospun poly lactic acid (PLA) fibres: effect of different solvent systems on fibre morphology and diameter, Polymer 55 (18) (2014) 4728–4737.

[31] J. Zhu, D. Tang, Z. Lu, Z. Xin, J. Song, J. Meng, J.R. Lu, Z. Li, J. Li, Ultrafast bone-like apatite formation on highly porous poly (l-lactic acid)-hydroxyapatite fibres, Mater. Sci. Eng. C 116 (2020) 111168.
[32] Z. Ma, M. Kotaki, T. Yong, W. He, S. Ramakrishna, Surface engineering of electrospun polyethylene terephthalate (PET) nanofibers towards development of a new material for blood vessel engineering, Biomaterials 26 (15) (2005) 2527–2536.
[33] T. Xu, X. Zhang, X. Dai, Properties of electrospun aligned poly (lactic acid)/collagen fibers with nanoporous surface for peripheral nerve tissue engineering, Macromol. Mater. Eng. 307 (10) (2022) 2200256.
[34] N. Wu, S. Lang, H. Zhang, M. Ding, J. Zhang, Solvent-induced crystallization behaviors of PLLA ultrathin films investigated by RAIR spectroscopy and AFM measurements, J. Phys. Chem. B 118 (44) (2014) 12652–12659.
[35] P. Pan, B. Zhu, W. Kai, T. Dong, Y. Inoue, Effect of crystallization temperature on crystal modifications and crystallization kinetics of poly (L-lactide), J. Appl. Polym. Sci. 107 (1) (2008) 54–62.
[36] J.D. Hartgerink, E. Beniash, S.I. Stupp, Self-assembly and mineralization of peptide-amphiphile nanofibers, Science 294 (5547) (2001) 1684–1688.
[37] D.L. Donovan, S.P. Schmidt, S.P. Townshend, G.O. Njus, W.V. Sharp, Material and structural characterization of human saphenous vein, J. Vasc. Surg. 12 (5) (1990) 531–537.
[38] M. Stekelenburg, M.C. Rutten, L.H. Snoeckx, F.P. Baaijens, Dynamic straining combined with fibrin gel cell seeding improves strength of tissue-engineered small-diameter vascular grafts, Tissue Eng. A 15 (5) (2009) 1081–1089.
[39] H. Yamada, F. Evans, Mechanical properties of circulatory organs and tissues, Strength Biol. Mater. (1970) 106–137.
[40] A.P. Rickel, X. Deng, D. Engebretson, Z. Hong, Electrospun nanofiber scaffold for vascular tissue engineering, Mater. Sci. Eng. C 129 (2021) 112373.
[41] S. Bai, J. Zhang, Y. Gao, X. Chen, K. Wang, X. Yuan, Surface Functionalization of electrospun scaffolds by QK-AG73 peptide for enhanced interaction with vascular endothelial cells, Langmuir (2023).
[42] H.J. Salacinski, S. Goldner, A. Giudiceandrea, G. Hamilton, A.M. Seifalian, A. Edwards, R.J. Carson, The mechanical behavior of vascular grafts: a review, J. Biomater. Appl. 15 (3) (2001) 241–278.
[43] B. Li, B. Liu, Y. Fu, O. Bondarenko, A. Verdant, O. Rochette-Drouin, J. Lin, J.-M. Bourget, R. Guzman, L. Wang, A floating thrombus anchored at the proximal anastomosis of a woven thoracic graft mimicking a genuine aortic dissection, J. Long Term Eff. Med. Implants 25 (3) (2015).
[44] J.M. Flack, B. Adekola, Blood pressure and the new ACC/AHA hypertension guidelines, Trends Cardiovasc. Med. 30 (3) (2020) 160–164.
[45] Y. Snyder, Q. Lasley, S. Jana, Vascular graft with native-like mechanical properties, Mater. Lett. 333 (2023) 133568.
[46] Y. Dong, S. Liao, M. Ngiam, C.K. Chan, S. Ramakrishna, Degradation behaviors of electrospun resorbable polyester nanofibers, Tissue Eng. B Rev. 15 (3) (2009) 333–351.
[47] D. Zhang, J. Chang, Electrospinning of three-dimensional nanofibrous tubes with controllable architectures, Nano Lett. 8 (10) (2008) 3283–3287.
[48] S. Eom, S.M. Park, H. Hong, J. Kwon, S.-R. Oh, J. Kim, D.S. Kim, Hydrogel-assisted electrospinning for fabrication of a 3D complex tailored nanofiber macrostructure, ACS Appl. Mater. Interfaces 12 (46) (2020) 51212–51224.
[49] Y. Si, J. Yu, X. Tang, J. Ge, B. Ding, Ultralight nanofibre-assembled cellular aerogels with superelasticity and multifunctionality, Nat. Commun. 5 (1) (2014) 5802.
[50] S. Fleischer, D.N. Tavakol, G. Vunjak-Novakovic, From arteries to capillaries: approaches to engineering human vasculature, Adv. Funct. Mater. 30 (37) (2020) 1910811.
[51] H. Zhong, J. Huang, J. Wu, J. Du, Electrospinning nanofibers to 1D, 2D, and 3D scaffolds and their biomedical applications, Nano Res. 15 (2) (2022) 787–804.
[52] L. Bao, F.F. Hong, G. Li, G. Hu, L. Chen, Improved performance of bacterial nanocellulose conduits by the introduction of silk fibroin nanoparticles and heparin for small-caliber vascular graft applications, Biomacromolecules 22 (2) (2020) 353–364.
[53] M.F. Leong, K.S. Chian, P.S. Mhaisalkar, W.F. Ong, B.D. Ratner, Effect of electrospun poly (d, l-lactide) fibrous scaffold with nanoporous surface on attachment of porcine esophageal epithelial cells and protein adsorption, J. Biomed. Mater. Res. A 89 (4) (2009) 1040–1048.
[54] S. Anoopkumar-Dukie, J. Carey, T. Conere, E. O'sullivan, F. Van Pelt, A. Allshire, Resazurin assay of radiation response in cultured cells, Br. J. Radiol. 78 (934) (2005) 945–947.